Multi-wavelength detection of an ongoing FUor-type outburst

Zhen Guo[1,2,3,4]★, P. W. Lucas[4], R. G. Kurtev[1,5], J. Borissova[1,5], Vardan Elbakyan[6,7], C. Morris[4], A. Bayo[8], L. Smith[9], A. Caratti o Garatti[10,11], C. Contreras Peña[12,13], D. Minniti[14,15,16], J. Jose[17], M. Ashraf[17], J. Alonso-García[18,5], N. Miller[4], and H. D. S. Muthu[4]

[1]*Instituto de Física y Astronomía, Universidad de Valparaíso, ave. Gran Bretaña, 1111, Casilla 5030, Valparaíso, Chile*
[2]*Núcleo Milenio de Formación Planetaria (NPF), ave. Gran Bretaña, 1111, Casilla 5030, Valparaíso, Chile*
[3]*Departamento de Física, Universidad Tecnicá Federico Santa María, Avenida España 1680, Valparaíso, Chile*
[4]*Centre for Astrophysics Research, University of Hertfordshire, Hatfield AL10 9AB, UK*
[5]*Millennium Institute of Astrophysics, Nuncio Monseñor Sotero Sanz 100, Of. 104, Providencia, Santiago, Chile*
[6]*Fakultät für Physik, Universität Duisburg-Essen, Lotharstraße 1, D-47057 Duisburg, Germany*
[7]*Research Institute of Physics, Southern Federal University, Stachki Ave. 194, Rostov-on-Don 344090, Russia*
[8] *European Organisation for Astronomical Research in the Southern Hemisphere (ESO), Karl-Schwarzschild-Str. 2, 85748 Garching bei München, Germany*
[9]*Institute of Astronomy, University of Cambridge, Madingley Road, Cambridge, CB3 0HA, UK*
[10]*INAF - Osservatorio Astronomico di Capodimonte, salita Moiariello 16, 80131, Napoli, Italy*
[11]*Dublin Institute for Advanced Studies, School of Cosmic Physics, Astronomy and Astrophysics Section, 31 Fitzwilliam Place, Dublin 2, Ireland*
[12]*Department of Physics and Astronomy, Seoul National University, 1 Gwanak-ro, Gwanak-gu, Seoul 08826, Republic of Korea*
[13]*Research Institute of Basic Sciences, Seoul National University, Seoul 08826, Republic of Korea*
[14]*Departamento de Ciencias Fisicas, Universidad Andres Bello, Republica 220, 8320000 Santiago, Chile*
[15]*Vatican Observatory, V00120 Vatican City State, Italy*
[16]*Departamento de Física, Universidade Federal de Santa Catarina, Trindade 88040-900, Florianopolís, SC, Brazil*
[17]*Indian Institute of Science Education and Research (IISER) Tirupati, Rami Reddy Nagar, Karakambadi Road, Mangalam (PO), Tirupati 517 507, India*
[18]*Centro de Astronomía (CITEVA), Universidad de Antofagasta, Av. Angamos 601, 02800 Antofagasta, Chile*

Accepted XXX. Received YYY; in original form ZZZ

ABSTRACT

Mass accretion during the star formation process is highly unstable, as Young stellar objects (YSOs) assemble most of their mass during the episodic accretion process. As the most outstanding eruptive events on young (proto)stars, the rarely seen FUor-type events (FUors) are valuable laboratories to investigate the outbursting nature of YSOs. Here, we present multi-wavelength detection of a pre-main-sequence (PMS) FUor-type object with an ongoing outburst, including optical to mid-infrared time series and near-infrared spectra. The initial outburst has an exceptional amplitude of >6.3 mag in *Gaia* and 4.6 mag in K_s, with a peak luminosity up to 16 $L_\odot$ and a peak mass accretion rate of 1.4×10^{-5} $M_\odot$ yr^{-1}. The optical to infrared spectral energy distribution (SED) of this object is consistent with a low-mass star ($0.2M_\odot$) with a modest extinction ($A_V < 2$ mag). A 100-d delay between optical and infrared rising stages is detected, suggesting an outside-in origin of the instability. The spectroscopic features of this object reveal a self-luminous accretion disc, very similar to FU Orionis, with a low line-of-sight extinction. Most recently, there has been another gradual increase in brightness throughout the wavelength range, possibly suggesting an enhancement of the mass accretion rate.

Key words: stars: pre-main sequence – stars: protostar – stars: variables: T Tauri – infrared: stars – accretion

1 INTRODUCTION

A FUor-type event, named after the prototype FU Orionis, displays a prominent outburst in its light curve, usually with an amplitude larger than 5 mag in the optical (see the review from Fischer et al. 2022). These events are rarely detected, as once per 10^4 to 10^5 years per YSO, estimated by the total known eruptive samples (Scholz 2012; Hillenbrand & Findeisen 2015; Contreras Peña et al. 2019, and Contreras Peña submitted). So far, only two dozen such events have been confirmed by photometric and spectroscopic data on disc-bearing Class II YSOs. More recently, this phenomenon has been observed at all stages and stellar masses in star formation, especially among embedded protostars (Contreras Peña et al. 2017a). Most FUor-type outbursts share two common photometric signatures (Hartmann & Kenyon 1996), high amplitude (~5 mag in optical) and long duration (tens to nearly one hundred years). These two characteristics distinguish FUors from the low-amplitude (up to a few mags) and short-timescale (up to a few years) events, such as EXor-type outbursts (Herbig 2007). Theoretical models have been proposed to trigger episodic accretion bursts on YSOs, including gravitational instabilities (GI, Armitage et al. 2001; Kratter & Lodato 2016), thermal instability (Lodato & Clarke 2004; Clarke et al. 2005), magneto-

★ E-mail: zguo@npf.cl

rotational instabilities (MRI, e.g. Zhu et al. 2009b; Elbakyan et al. 2021), disc fragmentation (e.g. Vorobyov & Basu 2015), stellar fly-by (Borchert et al. 2022) and evaporation of gas giant planets (Nayakshin et al. 2023).

During the FUor event, unlike the steady magnetospheric accretion seen on most disc-bearing YSOs, the disc material is directly accreted onto the star by the boundary layer accretion mode (Audard et al. 2014). The mass accretion rate during a solar mass FUor-type outburst can reach $10^{-4} M_{\odot}\mathrm{yr}^{-1}$, orders of magnitudes higher than the steady accretion stage. Episodic accretion models predict that most of the stellar mass is accumulated during these outbursts (Hartmann & Kenyon 1996). The released gravitational energy can efficiently heat the inner accretion disc, which becomes self-luminous and outshines the photospheric emission (Zhu et al. 2009a; Liu et al. 2022). The near-infrared (NIR) spectra of FUors resemble a bright but cool object, with strong absorption bands mainly from the molecules in the circumstellar disc/envelope. Most FUors are confirmed by a combination of eruptive photometric light curves along with their unique spectral features (Connelley & Reipurth 2018; Guo et al. 2021).

The eruptive behaviours of FUors across different wavelength ranges can provide clues on the origin of the triggering instability (Vorobyov et al. 2021). For instance, Gaia17bpi had a pre-outburst in the mid-infrared, 500 days before the optical outburst (Hillenbrand et al. 2018), indicating an outside-in propagation of the MRI originated at ~1 AU (Cleaver et al. 2023). In contrast, slow-rising outbursts in both optical and infrared bands are explained by inside-out propagating instabilities (e.g. Lin et al. 1985). Theoretical models predict months-long delays in the mid-IR light curves when the outburst is triggered by thermal instabilities initiated at several stellar radii from the star (Nayakshin & Elbakyan 2023). The fading stage of FUors contains information about the cooling efficiency of the viscous heated accretion disc. **Although the prototypes of FUors have stayed on their photometric plateau for decades, some recently discovered FUors have diverse photometric behaviours, such as the rapid-fading stages.** Previous studies preferred the enhancement of line-of-sight extinction as the explanation of the post-outburst rapid decays (Kopatskaya et al. 2013; Hackstein et al. 2015). However, analytical disc models suggest that the rapid cooling of the accretion disc can result in such decay in the brightness (Szabó et al. 2021; Carvalho et al. 2023).

Lucas et al. (submitted, hereafter LSG23) discovered 222 high-amplitude objects ($\Delta K_s > 4$ mag) from the decade-long Vista Variables in the Via Lactea survey (VVV, Minniti et al. 2010; Saito et al. 2012; Minniti 2016). In this work, we present multi-wavelength light curves and spectra of an ongoing FUor-type outburst (L222_78, RA: 17:18:19.65 Dec: -32:22:53.11) from the catalogue provided by LSG23. This object exhibited a high-amplitude eruptive stage (> 6.3 mag in *Gaia* G-band), followed by a rapid fading stage right after the initial outburst and a unique recent brightening across the wavelength spectrum.

2 OBSERVATION AND DATA REDUCTION

The eruptive behaviour of L222_78 was originally discovered in LSG23 using the K_s time series from the VVV Infrared Astrometric Catalogue (VIRAC2β, Smith et al. 2018, and in prep). The VIRAC2β catalogue provides PSF (point-spread function) photometry of dozens of K_s detections (from 2010 to 2019) and two multi-colour (Z, Y, J, H) epochs. A few epochs at/after the photometric maximum are saturated in the VVV images, which were corrected by custom-designed aperture photometry in LSG23.

In 2021 and 2022, we obtained single-epoch J, H, K_s photometry of this target using the Son of ISAAC infrared imager on the ESO NTT telescope (SOFI Moorwood et al. 1998). We obtained optical to NIR photometry from the SMARTS 1 m telescope in 2022 and the Rapid Eye Mount (REM) telescope in 2023. Two epochs of r and i-band images are found in the LCO science archive (Brown et al. 2013). Plus, we retrieved g, r, and i-band images of the *VPHAS+* survey taken by the VLT Survey Telescope (VST) from the ESO archive (Drew et al. 2014), and broadband calibrated images from *ATLAS* forced photometry server (Tonry et al. 2018a). Custom-designed aperture photometry measurements were applied to extract the brightness (see Guo et al. 2018).

We retrieved optical light curves and astrometry data from *Gaia* DR3 (Gaia Collaboration et al. 2016, 2023). Since this object is not included in the Gaia Photometric Science Alert, the archived data only includes observations up until circa 2017. The *Gaia* parallax measurement of L222_78 is 0.9209±0.0218 mas, which is equivalent to a distance of 1.08±0.02 kpc.

We obtained mid-infrared photometric data from *ALLWISE* (Wright et al. 2010) and *NEOWISE* (Mainzer et al. 2014) surveys via the NASA/IPAC Infrared Science Archive. Due to the low spatial resolution, L222_78 is blended with a nearby companion (d = 2.2”, **likely to be a background post-MS source, see Appendix**). We performed custom-written PSF photometry on these two sources, using the epoch-binned *unWISE* images (Lang 2014; Meisner et al. 2017), obtained from the online *wiseview* tool[1]. The PSF functions were generated in each image (2’ x 2’) by the DAOPHOT package, using the 30 brightest sources in the field (Stetson 1987). Then, the PSF function is applied to the target and companion with fixed central locations obtained from the VVV survey. Finally, we obtained the best-fit heights of the PSF functions for both sources using the least χ^2 method. The typical uncertainty around the photometric maximum is 0.1 mag and enhanced to 0.5 mag around the photometric minimum. There was no detection from *Spitzer*.

Two spectra of L222_78 were observed in 2021 and 2023. The XSHOOTER spectra (Vernet et al. 2011) were obtained on the Very Large Telescope on April 16th 2021. We used optical and NIR arms of the XSHOOTER with slit widths of 0.9” in the optical and 0.6” in the NIR, with exposure times of 210s and 300s, respectively. The data was reduced using the pipeline package built on the REFLEX platform (Freudling et al. 2013). We applied the MOLECFIT software to correct the telluric absorption and to generate wavelength solution of 2nd-order polynomial (Smette et al. 2015; Kausch et al. 2015). On May 9th 2023, we obtained NIR spectra from the Folded-port Infra-Red Echellette (FIRE) spectrograph on the Magellan Baade Telescope (Simcoe et al. 2013). The spectra are composed of four 90s exposures in the ABBA mode using the 0.6” slit. An A0-type telluric standard is obtained afterwards. We applied the FIREHOSE v2.0 pipeline to reduce the data (Gagne et al. 2015), using similar methods described in Guo et al. (2020).

3 RESULTS

3.1 Photometric features

The optical to infrared lightcurves of L222_78, from 2010 to 2023, are presented in Figure 1. We divide the entire eruptive event into four stages based on the light curve morphology: the pre-eruptive pre-outbursting stage, the rising stage, the post-peak decaying stage

[1] http://byw.tools/wiseview

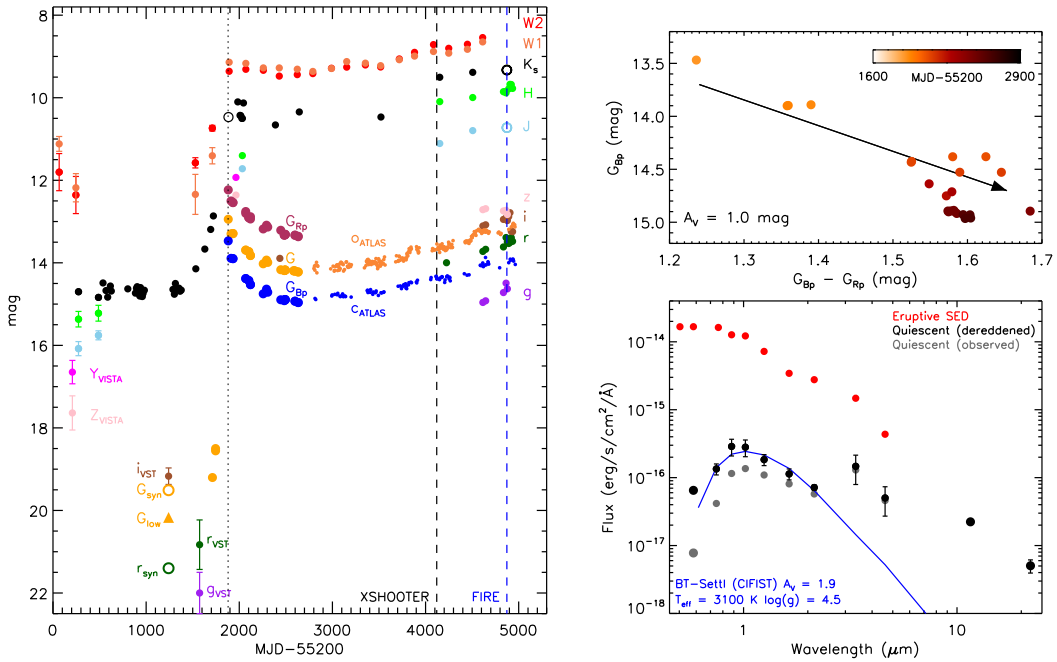

Figure 1. *Left*: Multi-wavelength light curves of L222_78, colour coded by photometric bands. Error bars less than 0.1 mag are not shown. Open symbols are synthetic magnitudes computed from the SED best-fitting atmospheric model and spectra, respectively. Vertical dashed lines mark the observation dates of two spectral epochs. The ending point of the rising stage is shown by the dotted line (around MJD 57080/2015-02-27). *Upper Right*: Gaia colour-magnitude diagram with an extinction vector (A_V = 1.0 mag) adopted from Wang & Chen (2019). The data points are colour-coded by the observation time. *Lower Right*: The pre-outbursting (grey), dereddened (black) and eruptive (red) SEDs. A BT-Settl model is fit to the pre-outbursting SED assuming A_V = 1.9 mag (blue).

and the re-brightening stage. The K_s (VVV and SOFI) and *WISE* photometry are obtained throughout all stages, and the post-eruptive decaying stage is well-covered by *Gaia* light curves. Several sparse multi-colour photometry (g, r, i and *VISTA* filters) are obtained at both pre-outbursting and post-eruptive stages, which are applied to measure the spectral energy distribution (SED) of the target.

The rising stage of the outburst started in **Oct 2013 and reached the peak brightness before MJD 57080 (Feb 2015)**, captured by the *WISE* and *Gaia* data. In the optical, the outburst has an exceptionally fast eruptive stage, as $\Delta G > 6.3$ mag within 170 days, resembling the behaviour of FU Ori. The first *Gaia* epoch was 338 days after the beginning of the near-infrared outburst. Nevertheless, a lower limit of the pre-outbursting G magnitude ($G_{\rm low}$) is estimated by the photometric transformation equation as 20.17 mag[2], and a higher value is found from the synthetic photometry of the best fitting photospheric model (see 3.2). The duration of the eruptive stage across different bands will be further addressed by analytical functions in §3.3.

After reaching the photometric maximum, the **Gaia** light curves of L222_78 entered a decaying stage, whilst the infrared brightness remained relatively constant. We present the G_{Bp} and G_{Rp} colour-magnitude diagram in Figure 1. The **optical decay** is consistent with the extinction law with R_V = 3.1 and A_V = 1.0 mag (Wang & Chen 2019). Based on the *Gaia* light curves, we generated a time-extinction correlation to reconstruct the peak brightness in VVV filters. The variation of extinction is not unusual on FUors, which is often referred to as the temporary dusty structure piled up near/at the innermost accretion disc, or the dust lifted by the outflow during the ejection outburst. For instance, V1057 Cyg, one of the prototypes of FUors, **faded ~2 mag in 3 years** after reaching the peak (Herbig 1977). The post-peak enhancement of A_V has been confirmed in several **FUors**, including **HBC722**, V960 Mon, Gaia21bty and V2493 Cyg (Kóspál et al. 2011; Hackstein et al. 2015; Siwak et al. 2023; Ghosh et al. 2023).

A low-amplitude colour-less brightening trend is detected in the *ATLAS* light curves (see Figure 1 and Appendices), which is opposed to the extinction law mentioned above. The same rising trend is detected in the mid-infrared, indicating a piling up of warm material in the circumstellar disc, which resembles the behaviour of PGIR 20dci (Hillenbrand et al. 2021). However, in the latter case, there was a secondary outburst a decade after the primary outburst, which has not happened yet on L222_78. Nevertheless, we observe a change in the slope of the NIR continuum spectra, which can be interpreted as variable extinction (see §3.4). Therefore, we conclude that the **recent** rising trend on L222_78 is likely attributed to a mixture of increasing mass accretion rate and clearing of line-of-sight extinction. The enhancement in the mid-infrared brightness also suggests the existence of warm dust in the circumstellar disc.

3.2 SED and bolometric luminosity

We present the pre-outburst and outbursting SEDs of L222_78 using photometric data obtained between 0.5 to 22 μm. The pre-outbursting SED comprises VVV photometry taken in 2010, the *VPHAS+ i*-band in 2013 and *WISE* bands from our PSF photometry. We assume no significant variability ($\Delta m > 0.5$ mag) during the pre-outbursting stage. **In the following SED fitting procedure, the $W3$ and $W4$-band magnitudes from the *ALLWISE* survey are treated as upper limits, as there are other faint sources located within the *WISE* beam. However, judging by the central location of the WISE de-**

[2] According to the *Gaia* EDR3 document, $G - g < -(g - i) + 1.0$

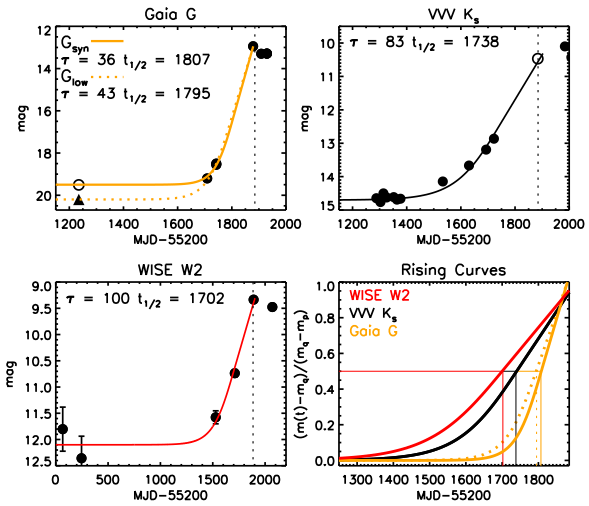

Figure 2. Rising light curves of L222_78, including synthetic brightness from SEDs (open circles) and lower limit in G (triangle). Analytical functions are fit for each band. The normalised curves are shown in the bottom right with $t_{1/2}$ marked out. The ending of the raising stage is marked by the dashed vertical lines in each light curve plot.

tections, L222_78 should be the dominant contributor in $W3$- and $W4$-band fluxes. For the in-outburst (peak) brightness, we adopted *Gaia* and *NEOWISE* detection at/near the photometric maximum. The VVV magnitudes were measured ~100 days after the photometric maximum, which was affected by the enhancement of the extinction. Hence, the peak VVV magnitudes were estimated by correcting the extinction estimated from the *Gaia* light curves (see §3.1). We then performed a least-χ^2 fitting of the pre-outbursting SED to BT-Settl models (Barber et al. 2006; Caffau et al. 2011; Allard et al. 2011) using the VOSA tool (Bayo et al. 2008) with a fixed Gaia distance (1.08 kpc) and A_V ranging between 0 to 5 mag.

The pre-outbursting SED fitting result suggests that the progenitor has an effective temperature of 3100 K (1σ confidence: 2769 - 3373 K) and a bolometric luminosity, $L_{\rm bol} = 0.16 \pm 0.02\ L_\odot$. Although the stellar luminosity is a lower limit as there was barely any photospheric emission having been detected. The star could be heavily embedded and therefore be intrinsically bluer and more massive. From the best fitting photosphere to the pre-outbursting SED, we compute the synthetic magnitude in G and r during the pre-outbursting stage, as $G_{\rm syn} = 19.5$ mag and $r_{\rm syn} = 21.4$ mag. Accurate measurements of the $L_{\rm bol}$ at the outbursting stage rely on the precise estimation of A_V. The post-outbursting spectra suggest very low extinction, with $A_V < 1$ mag (see §3.4). Therefore, the outbursting bolometric luminosity is between 9 to 16 $L_\odot$ when assuming A_V ranging between 0 to 1 mag. Under the assumption that the accretion luminosity ($L_{\rm acc}$) is roughly equal to the bolometric luminosity during the eruptive stage, we estimated the peak mass accretion rate ($\dot{M}_{\rm acc}$) is 0.8 to 1.4 $\times\ 10^{-5}\ M_\odot\ {\rm yr}^{-1}$, by simply applying an approximated correlation, $\dot{M}_{\rm acc} = L_{\rm acc} R_* / (G M_*)$, (Gullbring et al. 1998). **The peak absolute brightness of this source ($M_G \sim 3$ mag, adopting the Gaia distance) rules out the possibility of this source being a stellar merger candidate. According to Karambelkar et al. (2023), most stellar mergers have absolute magnitudes brighter than -3 mag in optical.**

3.3 Rising Timescale

The rising stage of L222_78 was captured by a broad wavelength range, including an exceptional optical amplitude ($\Delta G > 6.3$ mag) which places it as one of the highest amplitude eruptive events on YSOs. We applied analytical functions to describe the exponential rising stage in G, K_s, and $W2$ using observed and synthetic magnitudes. We adopted the two-step formalism originally designed by LSG23,

$$t < t_{1/2}: \quad m(t) = m_q - \frac{m_q - m_p}{1 + e^{-(t - t_{1/2})/\tau}} \tag{1}$$

$$t \geq t_{1/2}: \quad m(t) = m_q - (m_q - m_p)(0.5 + 0.5(t - t_{1/2})/2\tau) \tag{2}$$

where $t_{1/2}$ is the time when the brightness is enhanced by half of the amplitude and τ is a timescale parameter. Additionally, m_q and m_p are the pre-outbursting and peak magnitudes obtained from the time series which are treated as constants in our fitting. As designed, the photometric maximum (m_p) is reached at $t_{1/2} + 2\tau$, where the rising stage ends. This formalism reflects the classical rising morphology of most YSO outbursts in LSG23, composed of a slow-rising stage at the beginning that gradually accelerates before reaching a constant rate of brightening until reaching the photometric maximum.

Here, we used the photometric maxima captured by *Gaia* and *NEOWISE* near MJD 57083, and the synthetic peak magnitude in K_s (measured from the SED fitting above) as m_p. For m_q, we took the mean magnitude in K_s and $W2$ before MJD 56400, plus the $G_{\rm syn}$ and $G_{\rm lim}$ estimated in previous sections. We applied the χ^2 minimization method on two free parameters ($t_{1/2}$ and τ) with grid sizes of 1 day. The light curves, best-fitting analytical curves, and fitting parameters are presented in Figure 2. In most cases, the analytical functions fit the data well, except in K_s where the brightness increased slightly faster than the model in the first 200 days.

To compare the rising stages across different wavelengths, we present the normalised rising curves on the bottom right panel of Figure 2. We found that the choice of pre-outbursting magnitude, either $G_{\rm syn}$ or $G_{\rm lim}$, does not significantly affect the fitting results in G. The infrared bands ($W2$ and K_s) started rising earlier and reached the $t_{1/2}$ point 60 to 100 days quicker than the G-band. The curve in G is much steeper (smaller τ) than the infrared, indicating a faster-rising nature in optical **, with 170 days in the rising stage. However, this rising timescale is still much longer than the case of stellar mergers, which is on the order of 1 month (and they often fade quickly afterwards, Tylenda et al. 2011). The delay between the optical and infrared rising light curves agrees with the phenomenon predicted by the outside-in triggering mechanism of FUors (Cleaver et al. 2023). However, the time delay observed on L222_78 is five times shorter than the delays on Gaia17bpi and Gaia18dvy (about 500 days Hillenbrand et al. 2018; Szegedi-Elek et al. 2020).** Theoretically, the duration of the delay is consistent with the viscous timescale of the disc, proportional to the square root of the disc mass ($M_d^{0.5}$), which should be similar among low-mass YSOs. We will discuss the triggering mechanisms in §4.

3.4 Spectroscopic features

The optical spectrum of L222_78 is presented in the upper panel of Figure 3, which contains a forest of absorption features that are very similar to currently known FUors (Hillenbrand et al. 2023). The blueshifted $H\alpha$ absorption feature (-70 km/s) indicates a wind launched during the outburst, as a persistent property of FUors (see Audard et al. 2014). We find strong P Cygni profiles on Ca II, consistent with the spectral features of FUors (Hillen-

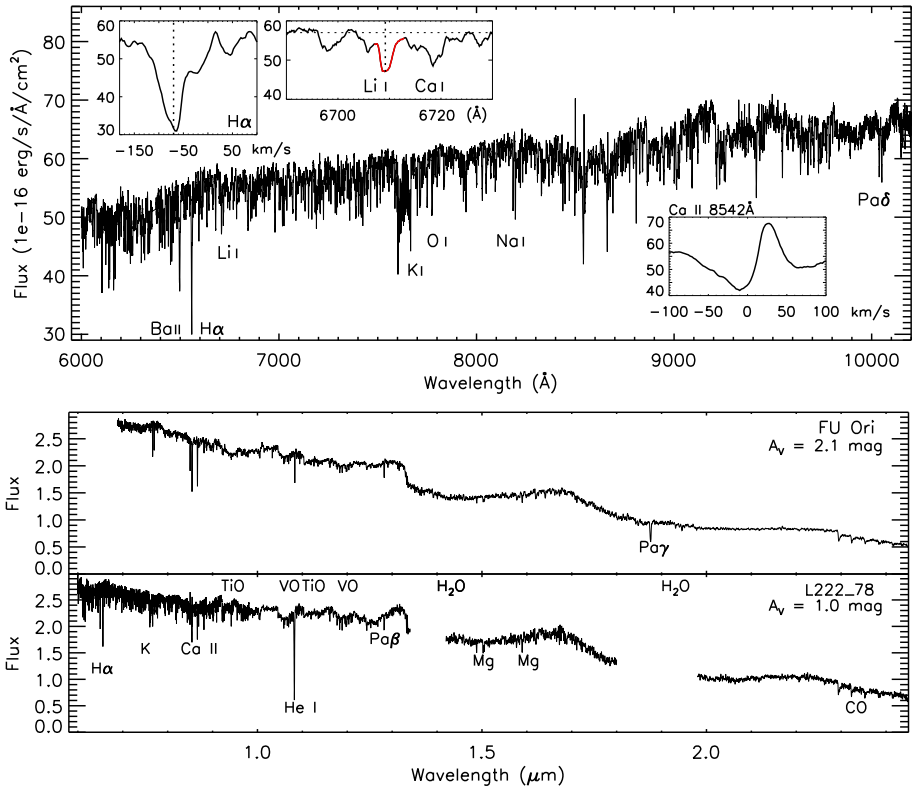

Figure 3. *Upper:* Optical spectrum of L222_78, with line profiles of $H\alpha$, Li I and Ca II absorption lines. *Lower*: Dereddened NIR spectra of FU Ori (IRTF; Connelley & Reipurth 2018) and L222_78 (XSHOOTER). Spectral features are marked individually on the plot.

brand et al. 2019; Szabó et al. 2021). We detected the Li λ6708Å absorption line (EW = 0.57 ± 0.08 **Å, integrated between 6707 to 6713Å), as a common indicator of a young age (e.g. Bayo et al. 2011; Campbell-White et al. 2023), and well matches the 1-2 Myr age estimation (Class II YSO). Plus, the spectral shape of the alkali lines (e.g. Na I lines at 818 nm) suggests log g > 4, instead of the low gravity post-MS AGB stars (more plots are presented in appendices). These optical spectral features also rule out the possibility of a candidate stellar merger, in which case the $H\alpha$ line is usually seen in emission (see Karambelkar et al. 2023).**

During a FUor-type event, the viscously heated inner accretion disc becomes more luminous than the stellar photosphere, hence a cool but bright spectrum is observed in the infrared (and a hotter **G/K**-type spectrum in the optical). In the infrared, the unique spectral absorption features of FUors often resemble cool dwarfs, such as the water vapour absorption arising from a low-gravity disc atmosphere, H I lines, deep He I absorption at 1.08 μm (typically associated with strong non-collimated winds), CO bandheads at 2.3 μm and many other molecular bands (e.g. VO, TiO; Connelley & Reipurth 2018). Notably, no jet/outflow feature (e.g. [Fe II], H_2) is detected. In the **lower** panel of Figure 3, we compared the dereddened XSHOOTER spectrum of L222_78 with the spectrum of FU Ori published in Connelley & Reipurth (2018). Both spectra exhibit similar features, although HeI absorption is much deeper on L222_78. Following the method applied in Connelley & Reipurth (2018), we estimated the line-of-sight extinction of L222_78 by aligning the H-bandpass continuum with FU Ori, as $A_V = 1.0$ mag.

We fit a theoretical model of the CO overtone emission ($\Delta v = 2$) to the bandheads between 2.32 and 2.38 μm. The model is initially designed in Contreras Peña et al. (2017b), with free parameters including effective temperature ($T_{\rm eff}$), column density of the CO molecule ($N_{\rm CO}$), and radial velocity (RV) of the system. The spectra from both epochs share almost identical features, with fitting results as RV = -10 ± 5 km/s, $T_{\rm eff} = 3500 \pm 500$ K, and $N_{\rm CO} = 1 \pm 0.1 \times 10^{-20}$ cm^{-2}.

Spectroscopic variability is detected between the two epochs and interpreted as variable extinction, **see a comparison between the two NIR spectra of L222_78 in the appendix. The difference in the spectral slope between the two epochs can be well-fitted by slightly modifying the line-of-sight extinction by $A_V = 1.2$ mag.** We measured $A_H = 0.16$ mag between the two spectra, which is smaller than the contemporary photometric variability ($\Delta H = 0.24$ mag). **The dereddened spectra of L222_78 show great similarity to the dereddened IRTF spectra of FU Ori, assuming $A_V = 2.1$ mag (Liu et al. 2022).** The low extinction estimated from our NIR spectra suggests that L222_78 should have recovered from the post-peak extinction event. **Compared with the estimated extinction in the pre-outburst SED ($A_V = 1.9$ mag), it is quite reasonable to assume that the outburst has cleared out the immediate line-of-sight extinction, also contributing to the high optical amplitudes.**

3.5 L222_78 as a young stellar object

L222_78 is located outside the coverage of the heritage archives of *Spitzer* satellite, and hence not classified as a YSO by *Spitzer*-based catalogues (e.g. Kuhn et al. 2021). We discovered the following evidence to support a pre-MS classification of L222_78. We found a few PGCC sources (Planck catalogue of Galactic cold clumps) located in the vicinity of this target, such as PGCC G354.18+02.87 (Planck Collaboration et al. 2016). With a spatial distance of 6', there is a young open cluster VdBH 221 with a very similar

parallax to L222_78 (0.88 Cantat-Gaudin & Anders 2020). Our SED models suggest $T_{\rm eff}$ ~3100 K and $L_{\rm bol} \sim 0.16 L_\odot$ during the pre-outburst stage, locating this target in the zone of pre-MS stars on the H-R diagram. According to evolutionary models (Baraffe et al. 2015), this target is a ~0.2 $M_\odot$ YSO with an age of 1-2 Myr and radius of 1.1 $R_\odot$. The pre-outburst NIR colour indices ($J-H = 0.71$ and $H-K_s$ = 0.43) are consistent with the intrinsic colours of Class II YSOs (Meyer et al. 1997). The infrared spectral slope (2 to 24 μm), known as the α-index (Lada 1987; Greene et al. 1994), also suggests L222_78 is a Class II YSO (α =-1.1). In the optical spectrum, we detected the Li absorption line, as a common indicator of young stars (see §3.4). Plus, the optical alkali lines are not consistent with a low-gravity source (i.e. AGB stars). We also note that, historically, not all eruptive YSOs have been detected in young stellar clusters. A few kinematically or spatially isolated FUors have been discovered, as such RNO 54 (Hillenbrand et al. 2023; Magakian et al. 2023).

4 DISCUSSION, REMARKS AND SUMMARY

This study presents an ongoing FUor-type object, L222_78, **with a 6.3 mag outburst observed in the Gaia time series and an optical rising stage of 170 days). The prevalence of absorption features in the optical to NIR spectra confirmed its FUor-type. The P Cygni profiles on Ca II lines indicate strong wind launched after the outburst.** A short time delay ($\Delta t_{1/2}$ = 100 days) is observed between the infrared and optical rising stages, suggesting an outside-in propagated instability that originated in the circumstellar disc at a radius around 0.1 AU.

In the scenario of magnetospheric-rotational activation at the dead zone (DZ+MRI, Armitage et al. 2001; Elbakyan et al. 2021; Nayakshin & Elbakyan 2023), the burst is thermally triggered when the mid-plane temperature exceeds the critical temperature of ~800 K. The disc at this location gets ionised, and the heatwave propagates inwards from beyond 0.2 AU. However, the predicted time delay is on the scale of 10^3 days, much longer than the delay observed on L222_78. Nevertheless, for a short time delay, the instability must be originated closer to the star (i.e. 0.07 AU; Liu et al. 2022).

Alternatively, an outside-in burst could be introduced by an embedded massive proto-planet, which modifies the thermal instability bursts by opening a gap and piling up material behind its orbit (TIP, Lodato & Clarke 2004; Nayakshin et al. 2023; Nayakshin & Elbakyan 2023). In this scenario, the outburst starts outside the planetary orbit (< 0.1 AU) and propagates inwards, creating a months-long time delay between the optical and infrared bands, consistent with the delay observed on L222_78. The predicted peak mass accretion rate is on the order of 10^{-5} $M_\odot$ yr^{-1}, similar to our measurements on L222_78. During the outbursting stage, the temperature of the surrounding proto-planetary material will become higher than its own temperature. As a result, the protoplanet can go through the "extreme evaporation" (EE) phase, during which it is disrupted thermally (TIP+EE model, Nayakshin et al. 2023).

After the initial outburst, a rise in the visual extinction ($A_V \sim 1$ mag) has been detected by the Gaia time series. This change in extinction could be caused by temporary circumstellar dust structures that form subsequent to the outburst, lifted by the strong wind launched from the ejection burst, consequently affecting the optical depth at shorter wavelengths. This extinction event has not changed the overall eruptive phenomenon observed in the Gaia light curves ($\Delta G > 6.3$ mag). This is unlike the rapid fading V1647 Ori-type objects, whose 5 mag outburst has completely faded in 1000 days. According to the most recent NIR spectra, the extinction has been cleared out in the past years.

We discovered a continuous brightening trend in recent years, from optical (1 mag) to mid-infrared (0.8 mag), indicating an increased emission of the system, likely attributed to the eruptive energy heating up the circumstellar disc. Theoretically, a secondary rise is predicted by both the aforementioned TIP+EE and DZ+MRI models, attributed to the feeding from the evaporated planetary atmosphere or the change in the mean molecular weight of the gas as Hydrogen is ionised (see details in Nayakshin & Elbakyan 2023).

Using VOSA we fit a grid of BT-Settl models to the pre-outbursting SED. The synthetic magnitudes derived from the best-fit model are $G_{\rm syn}$ = 19.5 and $r_{\rm syn}$ = 21.4 mag. Compared with the peak brightness, we measured ΔG = 6.6 mag and Δr = 8.6 mag, ranking L222_78 among the highest amplitude FUor-type outbursts. The clearing of extinction during the outburst could partially contribute to the optical amplitude. The SED fitting result indicates that L222_78 is a low-mass YSO (0.2 $M_\odot$) with a modest extinction (A_V = 1.9 mag). The peak mass accretion rate is estimated as up to 1.4×10^{-5} $M_\odot$ yr^{-1}, indicating ~ 40 Earth masses have been accreted since the beginning of the outburst. Remarkably, only a few FUors have been detected within a comparable mass range in the literature, such as V2775 Ori and V346 Nor (Caratti o Garatti et al. 2011; Kóspál et al. 2021). Both sources have relatively heavy and gravitational-unstable circumstellar discs ($M_d > 0.25 M_\star$), making them good candidates for GI-triggered outbursts. Future sub-mm observations are anticipated to measure the disc mass of L222_78, to unveil the underlying triggering mechanism. Currently, with a low foreground extinction, L222_78 (despite its distance) is an excellent target for high-resolution follow-up observation, to enable studies on the outbursting behaviours of FUors.

DATA AVAILABILITY

The WISE data underlying this article are publicly available at the IRSA server https://irsa.ipac.caltech.edu/Missions/wise.html. The SOFI, VVV and VST data are publicly available at the ESO archive http://archive.eso.org/cms.html. The VIRAC2β version of the VVV/VVVX light curves has not yet been publicly released but is available on request to the first author. The raw photometric data obtained by REM and SMART are available upon request. The Gaia light curves and photometric measurements are published on the ESA website (https://www.cosmos.esa.int/gaia). The ATLAS data is available via the webpage of the survey. Reduced spectra are provided at http://star.herts.ac.uk/~pwl/Lucas/GuoZ/VVVspec/.

ACKNOWLEDGEMENTS

We thank Prof M. Connolly for sharing the spectrum of FU Orionis originally taken by IRTF. ZG is supported by the ANID FONDECYT Postdoctoral program No. 3220029. ZG acknowledges support by ANID, – Millennium Science Initiative Program – NCN19_171. ZG, PWL, and CJM acknowledge support by STFC Consolidated Grants ST/R00905/1, ST/M001008/1 and ST/J001333/1 and the STFC PATT-linked grant ST/L001403/1. This work has made use of the University of Hertfordshire's high-performance computing facility (http://uhhpc.herts.ac.uk).

J.A.-G., J.B. and R.K. thank the support from ANID's Millennium Science Initiative ICN12_009, awarded to the Millennium In-

stitute of Astrophysics (MAS). J.A.-G. acknowledges support also from Fondecyt Regular 1201490. ACG acknowledges support from INAF-GOG "NAOMY: NIR-dark Accretion Outbursts in Massive Young stellar objects" and PRIN 2022 20228JPA3A - PATH. V.E. acknowledges the support of the Ministry of Science and Higher Education of the Russian Federation (State assignment in the field of scientific activity 2023, GZ0110/23-10-IF).

We gratefully acknowledge data from the ESO Public Survey program ID 179.B-2002 taken with the VISTA telescope, and products from the Cambridge Astronomical Survey Unit (CASU). This work contains data from ESO programs 105.20CJ and 109.233U, using SOFI on NTT and XSHOOTER on VLT. This research has made use of the NASA/IPAC Infrared Science Archive, which is funded by the National Aeronautics and Space Administration and operated by the California Institute of Technology. This work has made use of data from the European Space Agency (ESA) mission *Gaia* (https://www.cosmos.esa.int/gaia), processed by the *Gaia* Data Processing and Analysis Consortium (DPAC, https://www.cosmos.esa.int/web/gaia/dpac/consortium). Funding for the DPAC has been provided by national institutions, in particular, the institutions participating in the *Gaia* Multilateral Agreement. This paper includes data gathered with the 6.5 meter Magellan Telescopes located at Las Campanas Observatory, Chile. We acknowledge the support from the 1.0 m SMART telescope (operated by the SMARTS Consortium). This publication makes use of VOSA, developed under the Spanish Virtual Observatory project supported by the Spanish MICINN through grant AyA2008-02156.

REFERENCES

Allard F., Homeier D., Freytag B., 2011, in Johns-Krull C., Browning M. K., West A. A., eds, Astronomical Society of the Pacific Conference Series Vol. 448, 16th Cambridge Workshop on Cool Stars, Stellar Systems, and the Sun. p. 91 (arXiv:1011.5405)
Armitage P. J., Livio M., Pringle J. E., 2001, MNRAS, 324, 705
Audard M., et al., 2014, Protostars and Planets VI, pp 387–410
Baraffe I., Homeier D., Allard F., Chabrier G., 2015, A&A, 577, A42
Barber R. J., Tennyson J., Harris G. J., Tolchenov R. N., 2006, MNRAS, 368, 1087
Bayo A., Rodrigo C., Barrado Y Navascués D., Solano E., Gutiérrez R., Morales-Calderón M., Allard F., 2008, A&A, 492, 277
Bayo A., et al., 2011, A&A, 536, A63
Borchert E. M. A., Price D. J., Pinte C., Cuello N., 2022, MNRAS, 510, L37
Brown T. M., et al., 2013, PASP, 125, 1031
Caffau E., Ludwig H.-G., Steffen M., Freytag B., Bonifacio P., 2011, Sol. Phys., 268, 255
Campbell-White J., et al., 2023, A&A, 673, A80
Cantat-Gaudin T., Anders F., 2020, A&A, 633, A99
Caratti o Garatti A., et al., 2011, A&A, 526, L1
Carvalho A. S., et al., 2023, ApJ, 953, 86
Clarke C., Lodato G., Melnikov S. Y., Ibrahimov M. A., 2005, MNRAS, 361, 942
Cleaver J., Hartmann L., Bae J., 2023, MNRAS, 523, 5522
Connelley M. S., Reipurth B., 2018, ApJ, 861, 145
Contreras Peña C., et al., 2017a, MNRAS, 465, 3011
Contreras Peña C., et al., 2017b, MNRAS, 465, 3039
Contreras Peña C., Naylor T., Morrell S., 2019, MNRAS, 486, 4590
Drew J. E., et al., 2014, MNRAS, 440, 2036
Elbakyan V. G., Nayakshin S., Vorobyov E. I., Caratti o Garatti A., Eislöffel J., 2021, A&A, 651, L3
Fischer W. J., Hillenbrand L. A., Herczeg G. J., Johnstone D., Kóspál Á., Dunham M. M., 2022, arXiv e-prints, p. arXiv:2203.11257
Freudling W., Romaniello M., Bramich D. M., Ballester P., Forchi V., García-Dabló C. E., Moehler S., Neeser M. J., 2013, A&A, 559, A96
Gagne J., Lambrides E., Faherty J. K., Simcoe R., 2015, FireHose v2: Firehose v2.0, doi:10.5281/zenodo.18775, https://doi.org/10.5281/zenodo.18775
Gaia Collaboration et al., 2016, A&A, 595, A2
Gaia Collaboration et al., 2023, A&A, 674, A1
Ghosh A., et al., 2023, ApJ, 954, 82
Greene T. P., Wilking B. A., Andre P., Young E. T., Lada C. J., 1994, ApJ, 434, 614
Gullbring E., Hartmann L., Briceño C., Calvet N., 1998, ApJ, 492, 323
Guo Z., et al., 2018, ApJ, 852, 56
Guo Z., et al., 2020, MNRAS, 492, 294
Guo Z., et al., 2021, MNRAS, 504, 830
Hackstein M., et al., 2015, A&A, 582, L12
Hartmann L., Kenyon S. J., 1996, ARA&A, 34, 207
Herbig G. H., 1977, ApJ, 217, 693
Herbig G. H., 2007, AJ, 133, 2679
Hillenbrand L. A., Findeisen K. P., 2015, ApJ, 808, 68
Hillenbrand L. A., et al., 2018, ApJ, 869, 146
Hillenbrand L. A., et al., 2019, ApJ, 874, 82
Hillenbrand L. A., et al., 2021, AJ, 161, 220
Hillenbrand L. A., Carvalho A., van Roestel J., De K., 2023, arXiv e-prints, p. arXiv:2310.17227
Karambelkar V. R., et al., 2023, ApJ, 948, 137
Kausch W., et al., 2015, A&A, 576, A78
Kopatskaya E. N., Kolotilov E. A., Arkharov A. A., 2013, MNRAS, 434, 38
Kóspál Á., et al., 2011, A&A, 527, A133
Kóspál Á., et al., 2021, ApJS, 256, 30
Kratter K., Lodato G., 2016, ARA&A, 54, 271
Kuhn M. A., de Souza R. S., Krone-Martins A., Castro-Ginard A., Ishida E. E. O., Povich M. S., Hillenbrand L. A., COIN Collaboration 2021, ApJS, 254, 33
Lada C. J., 1987, in Peimbert M., Jugaku J., eds, IAU Symposium Vol. 115, Star Forming Regions. pp 1–17
Lang D., 2014, AJ, 147, 108
Lin D. N. C., Papaloizou J., Faulkner J., 1985, MNRAS, 212, 105
Liu H., et al., 2022, ApJ, 936, 152
Lodato G., Clarke C. J., 2004, MNRAS, 353, 841
Magakian T. Y., Movsessian T. A., Andreasyan H. R., Moiseev A. V., Uklein R. I., 2023, A&A, 675, A79
Mainzer A., et al., 2014, ApJ, 792, 30
Meisner A. M., Lang D., Schlegel D. J., 2017, AJ, 153, 38
Meyer M. R., Calvet N., Hillenbrand L. A., 1997, AJ, 114, 288
Minniti D., 2016, in Galactic Surveys: New Results on Formation, Evolution, Structure and Chemical Evolution of the Milky Way. p. 10
Minniti D., et al., 2010, New Astronomy, 15, 433
Moorwood A., Cuby J. G., Lidman C., 1998, The Messenger, 91, 9
Nayakshin S., Elbakyan V., 2023, MNRAS, submitted
Nayakshin S., Owen J. E., Elbakyan V., 2023, MNRAS, 523, 385
Planck Collaboration et al., 2016, A&A, 594, A28
Saito R. K., et al., 2012, A&A, 537, A107
Scholz A., 2012, MNRAS, 420, 1495
Simcoe R. A., et al., 2013, PASP, 125, 270
Siwak M., et al., 2023, MNRAS, 524, 5548
Smette A., et al., 2015, A&A, 576, A77
Smith L. C., et al., 2018, MNRAS, 474, 1826
Stetson P. B., 1987, PASP, 99, 191
Szabó Z. M., et al., 2021, ApJ, 917, 80
Szegedi-Elek E., et al., 2020, ApJ, 899, 130
Tonry J. L., et al., 2018a, PASP, 130, 064505
Tonry J. L., et al., 2018b, ApJ, 867, 105
Tylenda R., et al., 2011, A&A, 528, A114
Vernet J., et al., 2011, A&A, 536, A105
Vorobyov E. I., Basu S., 2015, ApJ, 805, 115
Vorobyov E. I., Elbakyan V. G., Liu H. B., Takami M., 2021, A&A, 647, A44
Wang S., Chen X., 2019, ApJ, 877, 116
Wright E. L., et al., 2010, AJ, 140, 1868
Zhu Z., Espaillat C., Hinkle K., Hernandez J., Hartmann L., Calvet N., 2009a, ApJ, 694, L64

Zhu Z., Hartmann L., Gammie C., 2009b, ApJ, 694, 1045

APPENDIX A: PHOTOMETRIC MEASUREMENTS

[Will be presented as online supplementary files]

In this section, we provide more information on the aperture photometry methods that were applied to extract the brightness of L222_78 from the raw images. Specifically, L222_78 was observed by *VST* but does not appear in the *VPHAS+* DR2 catalogue, hence we obtained the reduced images via the ESO archive. As mentioned in the main text, a companion is located 2.2" away from L222_78, which was brighter than our target during the pre-outbursting stage. In high spatial resolution images, e.g. from *VST* and *VISTA*, these two sources are well-distinguished. However, custom-written programs are necessary for low-resolution images where the two targets are blended. For the same reason, we downloaded more than 1700 reduced images from the *ATLAS* forced-photometry server (pixel size 1.86"), to obtain more reliable measurements than the pipeline-produced PSF photometry. Example images observed by *VISTA*, *VST* and *ATLAS* are presented in Figure A1.

We first extract the brightness of L222_78 from the images with high spatial resolutions (*VST* and *SMARTS*), using aperture photometry with an aperture size of 1.5". Three bright and non-saturated nearby sources are selected as reference stars, with their brightness obtained from the *ATLAS* all-sky stellar reference catalogue (Tonry et al. 2018b). We used the standard deviation of the background and the statistical noise to calculate the photometric errors. We also measured the brightness of the companion source, from both *VST* and *SMARTS* images, as $g = 22.03 \pm 0.60$ mag, $r = 18.40 \pm 0.03$ mag, $i = 15.60 \pm 0.02$ mag and $z = 13.53 \pm 0.02$ mag. In addition, we used the functions from Tonry et al. (2018a) to convert g, r, i-band magnitudes to *ATLAS* bands.

Before reducing the data from *REM* and *ATLAS*, we co-added individual images into 1-day bins, to increase the signal-to-noise ratio. On average, there are four to five images per day per bandpass. We then extracted the combined brightness of L222_78 and the companion using a larger aperture (see Figure A1). Finally, to obtain the brightness of L222_78, we subtracted the expected brightness of the companion (measured above) from the combined brightness. The light curves and colour-magnitude diagrams of the *ATLAS* data are presented in Figure A2. An overall colour-less rising morphology is seen between both bands, plus some short-timescale variations are detected in the $o_{\rm ATLAS}$-band. The colour variation disagrees with the extinction vector from Wang & Chen (2019).

APPENDIX B: SPECTROSCOPIC FEATURES

Here we present more details on the optical and infrared spectra of L222_78.

APPENDIX C: PHOTOMETRIC DATA

[Will be presented as online supplementary files] The photometric time series of L222_78 is presented in Table C1.

This paper has been typeset from a TEX/LATEX file prepared by the author.

Table C1. Photometric data on L222_78

Date (MJD)	Band	Telescope	mag	err (mag)	method
56909	G	Gaia	19.20	0.03	c
57078	G	Gaia	12.94	0.01	c
57078	$G_{\rm BP}$	Gaia	13.47	0.01	c
57078	$G_{\rm RP}$	Gaia	12.23	0.01	c
56774	g	VST	22.00	0.50	p
56441	r	VST	20.83	0.60	p
56441	i	VST	19.17	0.20	p
58001	$o_{\rm ATLAS}$	ATLAS	14.04	0.08	p
58013	$c_{\rm ATLAS}$	ATLAS	14.86	0.09	p
55408	Y	VISTA	16.64	0.28	p
55408	Z	VISTA	17.63	0.41	p
...	...	...	...	...	...

The full version of this table can be found in the online supplementary file. Method: c: data obtained directly from the catalogue. p: data reduced in this paper.

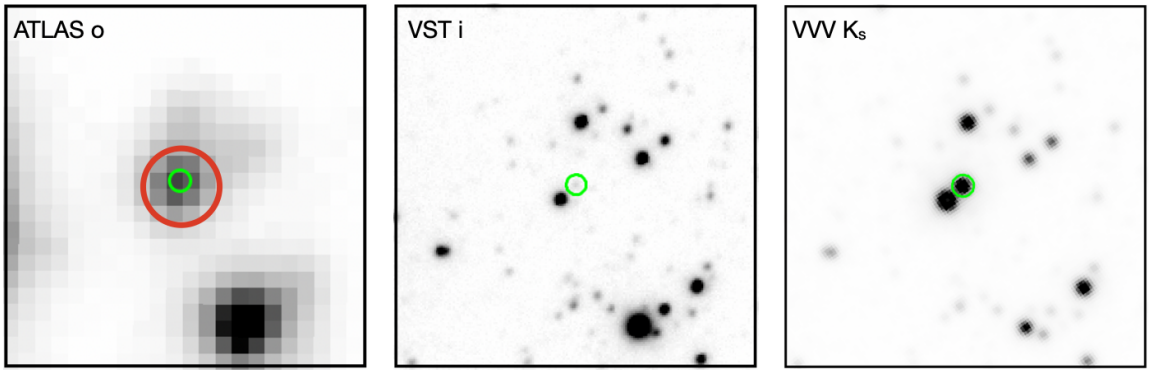

Figure A1. Photometric images of L222_78 from *ATLAS*, *VST* and the VVV survey. The size of the images is 40" × 40". The location of L222_78 is marked by the green circles with a radius of 1.2". The observation dates of the images are MJD 58007, MJD 56441 and MJD 57185, respectively. A larger aperture (5", red) is placed on *ATLAS* and *REM* images to include both L222_78 and its companion.

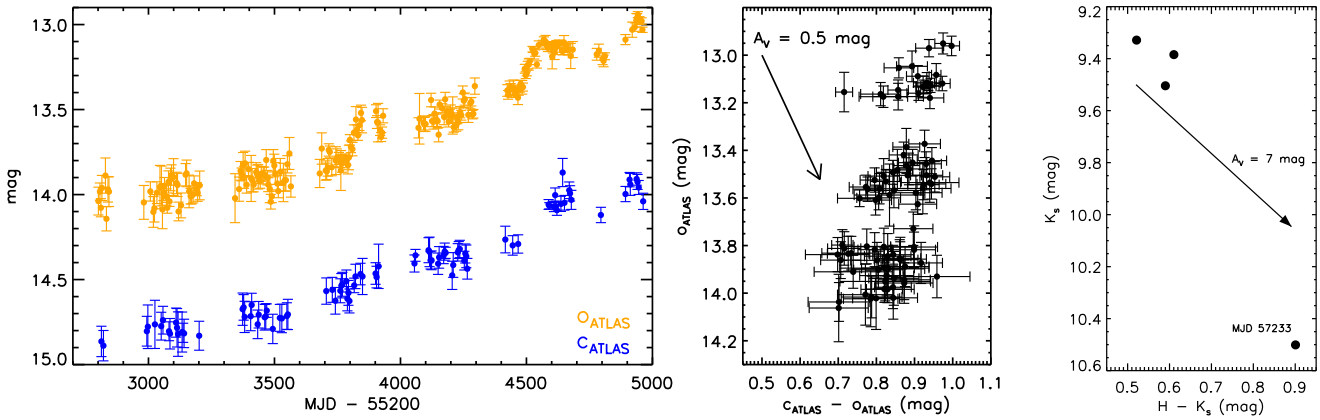

Figure A2. *Left*: *ATLAS* light curves of L222_78 during the post-decaying rising stage ($o_{\rm ATLAS}$: yellow, $c_{\rm ATLAS}$: blue). *Middle*: Colour magnitude diagram (CMD) of the *ATLAS* photometry. An extinction vector is presented with $A_V = 0.5$ mag. *Right*: Post-peak CMD of near-infrared bands. The data taken during the recent brightening stage is presented on the upper left corner.

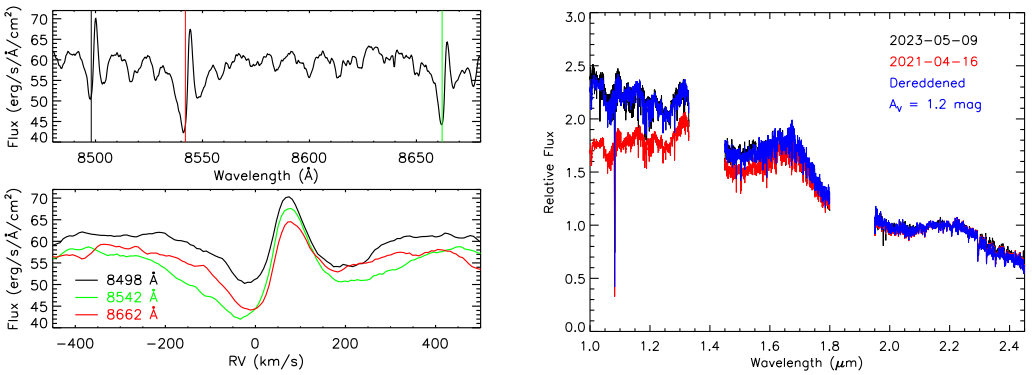

Figure B1. *Left*: Line profiles of three Ca II lines of L222_78. *Right*: spectra of L222_78 taken by FIRE (2023-05-09) and XSHOOTER (2021-04-16) spectrographs. The XSHOOTER spectrum is dereddened (blue) by $A_V = 1.2$ mag to match the continuum in the 2023 epoch.